Research Article | Vol. 12, No. 12 / 1 Dec 2021 / Biomedical Optics Express 7780
Biomedical Optics EXPRESS

Shot-noise limited tunable dual-vibrational frequency stimulated Raman scattering microscopy

SANDRO HEUKE,[1,5] INGO RIMKE,[2,5] BARBARA SARRI,[1,3] PAULINA GASECKA,[1] ROMAIN APPAY,[1,4] LOIC LEGOFF,[1] PETER VOLZ,[2] EDLEF BÜTTNER,[2] AND HERVÉ RIGNEAULT[1,3,*]

[1]*Aix Marseille Univ, CNRS, Centrale Marseille, Institut Fresnel, Marseille, France*
[2]*APE Angewandte Physik & Elektronik GmbH, Berlin, Germany*
[3]*Lightcore Technologies, Cannes, France*
[4]*APHM, CHU Timone, Service d'Anatomie Pathologique et de Neuropathologie, Marseille, France*
[5]*contributed equally to this work*
[*]*herve.rigneault@fresnel.fr*

Abstract: We present a shot-noise limited SRS implementation providing a >200 mW per excitation wavelength that is optimized for addressing two molecular vibrations simultaneously. As the key to producing a 3 ps laser of different colors out of a single fs-laser (15 nm FWHM), we use ultra-steep angle-tunable optical filters to extract 2 narrow-band Stokes laser beams (1–2 nm & 1–2 ps), which are separated by 100 cm^{-1}. The center part of the fs-laser is frequency doubled to pump an optical parametric oscillator (OPO). The temporal width of the OPO's output (1 ps) is matched to the Stokes beams and can be tuned from 650–980 nm to address simultaneously two Raman shifts separated by 100 cm^{-1} that are located between 500 cm^{-1} and 5000 cm^{-1}. We demonstrate background-free SRS imaging of C-D labeled biological samples (bacteria and *Drosophila*). Furthermore, high quality virtual stimulated Raman histology imaging of a brain adenocarcinoma is shown for pixel dwell times of 16 µs.

1. Introduction

Stimulated Raman scattering (SRS) is a fast micro-spectroscopy technique enabling scientist for label-free mapping of vibrational modes in inorganic and biological samples [1–4]. As the major advantage over coherent anti-Stokes Raman scattering (CARS), SRS is not compromised by the omnipresent non-resonant four-wave-mixing (FWM) signal and is, therefore, often referred to as "background"-free. It was soon discovered, however, that SRS-images are superimposed by other non-vibrational contrast mechanism such as cross-phase modulation (XPM), thermal lensing (TL) or two-photon absorption (TPA).

Over the past decade, various modifications of SRS-microscopy were presented that are suitable to reduce the background which we will review in the following. We shall find that these approaches are often either unnecessary complex, insufficient wavelength tunable, compromised by side effects or do not deliver suitable laser power levels to guarantee the highest possible imaging speed.

Berto et al. [5] implemented SRGOLD which balances the stimulated loss (SRL) and gain (SRG) process within a single SRS-channel by modulating, in a π-phase shifted manner, the superimposed signal and the idler beams of an optical parametric oscillator (OPO) [6]. The utility of SRGOLD is limited, however, to the Raman fingerprint region as large wavelength difference between the signal and idler beam are decreasingly well tolerated. Recently, we refined the concept of SRGOLD by modulating and demodulating both the pump and Stokes beam to detect SRL and SRG separately [7]. This technique, termed SRGAL, allows to measure and

#446348
Journal © 2021
https://doi.org/10.1364/BOE.446348
Received 18 Oct 2021; accepted 14 Nov 2021; published 24 Nov 2021

Biomedical Optics EXPRESS

balance SRS images at any vibrational resonance. Nevertheless, SRGAL comes at the expense of demodulating an already modulated beam which necessitates an elaborated electronic filtering.

SRGOLD and SRGAL both attempt to remove the background for a single Raman resonance. Alternatively, it is also possible to compare the SRS signal levels of silent spectral regions with the targeted resonant Raman modes. A sequential SRS-image acquisition at consecutive Raman shifts was achieved by Ozeki et al. [8] using galvo-scanners in combination with a grating to select a narrow-band seed pulse which is further power-amplified by a Yb-fiber. The galvo wavelength tuning is possible in the amplification profile of the Yb-fiber which leads to a rapid tuning over a 300 cm^{-1} spectral range. However, the sequential image acquisition limits this approach to immobile samples since, e.g., living organisms may move while changing the excitation wavelength so that an image subtraction for background removal becomes impossible. This issue is resolved when applying a simultaneous multi-spectral SRS image acquisition. The distinction between SRS-spectral channels can be achieved using a dispersive element as well as a detector array that is connected to multi-channel lock-in amplifier [9]. Alternatively, interferometry techniques proved to be less sensitive to linear scattering for signal demultiplexing [10]. As a third option, frequencies encoding with temporal modulations over a broadband excitation spectrum by an acousto-optical tunable filter (AOTF) enabled for multiplex-SRS for 3D investigations of *ex vivo* cutaneous mouse tissue [11]. To surpass the speed limitations a spatially-frequency modulation scheme was developed using laser scanners in combination with a grating and a mirror of laterally varying reflection [12]. All broadband fs-excitation approaches reported so far feature, however, low energy densities per spectral width ($\leq$ 10mW/nm) since either the samples damage threshold is reached, e.g. for 10 mW/nm and 10 nm FWHM spectral spread of the excitation, or the major part of the laser's output power is used to generate a second color severing as pump or Stokes beam.

Broadband fs-laser excitation certainly holds the advantage to address a large number of Raman bands but the investigation of only 2 deliberately selected Raman-bands (that we call here 'dual-color') already allows for a background minimization of comparable quality while the image acquisition speed can be boosted by orders of magnitude. On top of its potential for background free-image acquisition, dual-color SRS imaging [13–16] has been identified as a key approach to perform stimulated Raman histology where the simultaneous imaging of the CH_2 (2850 cm^{-1}) and CH_3 (2930 cm^{-1}) Raman shifts enables for the generation of virtual HE-images (hematoxylin and eosin) [17–20].

Meeting these considerations, a dual-color approach was introduced by Zhang et al. incorporating a grating together with an acousto-optic deflector employed as angle-to-wavelength pulse shaper [13]. As a disadvantage, the largest part of the fs-laser is wasted. Detecting two non-neighbouring Raman bands (off- or in-resonance), spectral focusing [22] in combination with two different time delays was implemented for dual-color SRS imaging [14]. However, any time delay between pump and Stokes pulses affect the optimal temporal overlap of the pulses and leads to a reduced signal generation. Alternatively, and to circumvent major drawbacks of the previously mentioned techniques, we recently introduced a dual-color SRS-microscopy approach combining the output of a fiber-laser at 1030 nm and two OPOs which are modulated at two distinct frequency to enable cross-talk-free SRS-imaging at two independently tunable Raman-shifts within the range of 500-5000cm^{-1} [16]. The performance of the latter is compromised by the utilization of a pump fiber-laser that is 6 dB(W) above the shot-noise limit at 20 MHz resulting in a decreased image acquisition speed. An auto-balanced detection [23] could in principle improve the performance of our system by 3dB(W) above the shot-noise, but would require still a 2$\times$ longer acquisition time as compared to a shot noise limited laser system. Besides speed, our dual-color SRS implementation [16] still requires two bulky and expensive OPOs which is not an option for the broad dissemination of the SRS technology.

Biomedical Optics EXPRESS

Here, we present a novel shot noise limited dual-color SRS laser system using a single OPO that enables for the simultaneous acquisition of two Raman shifts separated by ~ 100 cm^{-1}. Tuning the OPO's emission allows investigating Raman shifts within the range of 500–5000cm^{-1}. As the key-technology we use 4 ultra-steep edge-filters to split the output beam (FWHM ~ 100 cm^{-1}) of a low-noise fs solid state laser into 3 parts. The center part is frequency doubled and used to pump a tunable ps OPO which serves as pump for the SRS-process while two spectral parts neighboring the fs beam center are used directly as ps narrow band Stokes beams (Fig. 1(a). We exemplify this dual-color SRS laser source's potential for background removal as well as its spectral flexibility by imaging deuterated organisms (bacteria and *Drosophila*) simultaneously at there resonance (~ 2150 cm^{-1}) and off-resonance (~ 2050 cm^{-1}) Raman shifts. By imaging simultaneously CH_2 and CH_3 chemical bonds, we demonstrate virtual HE-imaging through a 0.5 mm thick adenocarcinoma within human brain tissue with an unprecedented combination of image quality and image acquisition speed for the laser power levels applied.

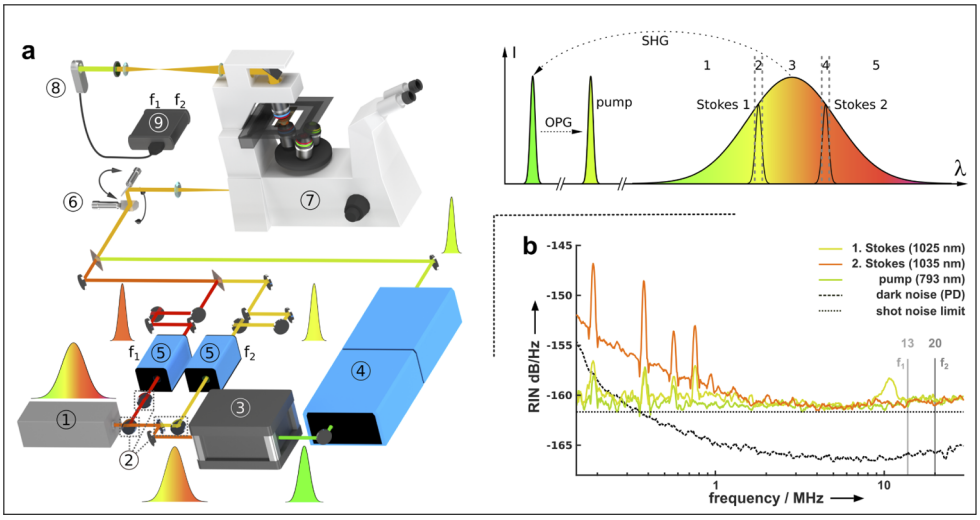

Fig. 1. Dual-color SRS experimental setup and laser noise: a) Setup - see the text for explanation. 1 passively mode-locked Yb fs-laser, 2 ultra-Steep angle-tunable filter, 3 second harmonic generation (SHG) unit, 4 OPO, 5 Electro-optic modulator (EOM), 6 Laser scanning mirrors, 7 Laser scanning microscope (LSM), 8 Photo-diode(s) (PD) with polarizing beam splitter, 9 Lockin-amplifier (LIA). b) Noise measurement: Above 1 MHz, the pump and the Stokes beams approach the shot noise limit at the relative intensity noise (RIN) level of −161.5 dB/Hz. The SRS noise measurement was performed following the protocol in reference [21]. Modulation frequencies of Stokes 1 and Stokes 2 beams are highlighted in grey at 13 MHz and 20 MHz.

2. Setup

A scheme of the experimental setup is shown in Fig. 1(a). As the main light source, we use a passively mode-locked fs-solid state-laser (LightConversion, FLINT, FL1-08) with a repetition frequency rate of 75.5 MHz, a central wavelength of 1030 nm and a spectral width of 15 nm (120 fs). The 8 W output of this fs-laser is split by 4 identical but differently angle-tuned ultra-steep long-pass filters (Semrock, LP02-1064RE-25) into 5 parts. The center part (3) of the laser comprising 4.2 W optical power is frequency doubled in a SHG unit featuring a spectral gain narrowing. The resulting 2.6 W at 515 nm are used to pump an optical parametric oscillator (OPO, APE Emerald) producing ps pulses. The 200 mW output power of the OPO serves as

Biomedical Optics EXPRESS

pump beam to activate the SRS-process. To address Raman resonances from 500–5000 cm^{-1} the OPO can be tuned from 650-980 nm with a spectral width of 1.1 nm at 793 nm (1 ps). Parts 2 and 4 of the fs-laser at 1025 nm and 1035 nm - see Fig. 1(a) - are used as Stokes beams and are modulated by electro-optical-modulators (EOM, APE, EOM 900) at 13 MHz and 20 MHz, respectively. Experimental data for the spectral and temporal width of the pump and Stokes beams can be found in the Supplement 1. Note that the unexploited spectral parts 1 and 5 still each contain 1.2 W. Exchanging the ultra-steep bandpass filter for suitable notch filter could further increase the efficiency of our approach.

Both Stokes as well as the pump beam are superimposed in time and space by delay stages and mirrors, and coupled into a home-built laser scanning microscope (LSM) [24]. To control the LSM we use the open-source LSM software ScanImage [25]. The 3 colors are jointly focused by an objective lens (Nikon, 40x, PLAN, NA = 1.15, immersion:water) onto the sample. Stimulated Raman loss (SRL) is detected by a 50 V reverse biased Photodiode (PD, APE SRS photodiode) collecting the OPO pump beam using a condenser lens (Nikon, C-C condenser Achromat/Aplanat, NA = 1.15, immersion:water). The Stokes beams are blocked before the PD (Semrock, FF01-950/SP-25). The SRS-signals are demodulated simultaneously by a dual-channel lock-in amplifier (SRS detection set dual, APE) at 13 MHz and 20 MHz generating two SRS-images of the two targeted Raman resonances which are defined by the frequency differences between pump and Stokes 1 as well as pump and Stokes 2.

3. Results

To maximize the SRS detection sensitivity or, equivalently, the imaging acquisition speed, the demodulated laser source must be shot-noise limited within the investigated bandwidth. Following the noise measurement protocol of Audier et al. [21] we assessed the shot-noise limited behavior of our SRS system. The results are shown in Fig. 1(b) and clearly confirm that the photon-noise dominates the power-spectral density of the pump and Stokes beams starting from 1 MHz.

To demonstrate the suitability of the dual-color SRS system for histopathology applications, we selected a sample of 1 mm^3 (0.5 mm thick) from an elderly patient operated for a rapidly progressive brain tumor. This sample was frozen and directly analyzed with the SRS system without micrometric sectioning, labelling or staining as usually done for conventional pathological examination. We performed SRS imaging at a sample depth of 20 µm while the SRS-signal was collected in the forward direction. 50% of the incident pump laser power was transmitted compared to a transparent sample, i.e. the object holder only. The results are displayed in Fig. 2. Note that the corresponding raw SRS image data can be found in SupFig. 3 within the Supplement 1. To retrieve the localization of nuclei the SRS-image at 2940 cm^{-1} is subtracted from a simultaneous acquired image at 2840 cm^{-1} and false-color-coded in purple to resemble the Hematoxylin stain. Mimicing Eosin, the SRS-image at 2840 cm^{-1} is stained in rose. The two images (2940 cm^{-1}-2840 cm^{-1}; 2840 cm^{-1}) together provide the stimulated Raman histology (SRH) image presented in Fig. 2 which readily serves pathologists for decision making by the evaluation of various morphological parameters such as the nuclei-to-cytoplasm ratio or cell density. It shall be noted that we recently established an excellent match between virtual SRH- and HE-images which were generated by conventional staining protocols [19].

To emphasize the clinical relevance of SRH imaging, the observations of a trained pathologist investigating Fig. 2 is summarized below: At low magnification (within Fig. 2), solid sheets of densely packed cells are observed presenting sharply demarcated margins with empty areas. Such a cellular architecture (i.e. cohesive interactions among cells) characterize tumors arising from epithelial cells. Further, a poorly formed glandular structure can be identified corresponding to the oval-shaped empty area within cells. At high magnification, it can be recognized signs of malignancy with prominent cellular atypia, increased nuclear-to-cytoplasmic ratio and nuclear

Biomedical Optics EXPRESS

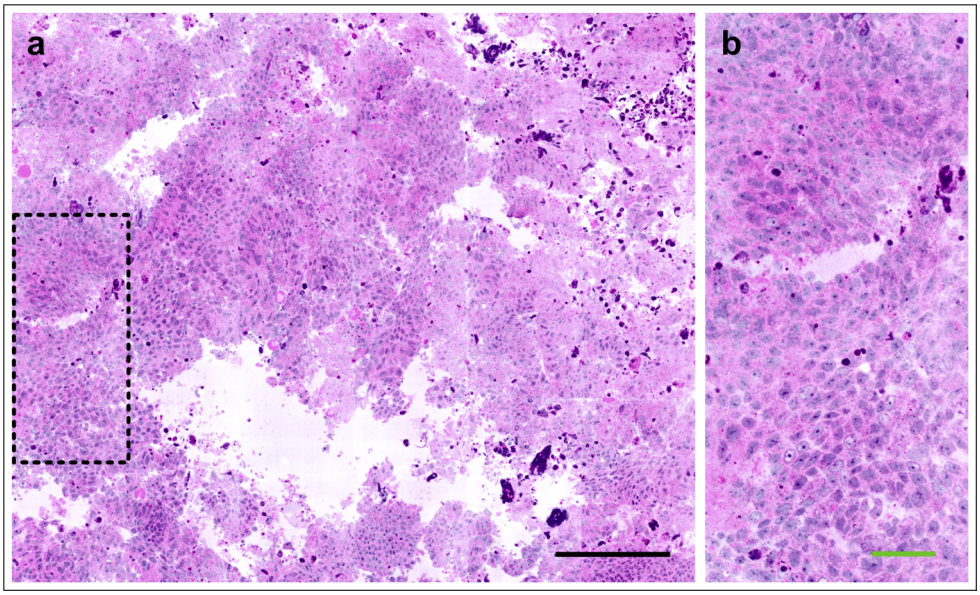

Fig. 2. Dual-color SRS applied to virtual stimulated Raman histology (SRH) of a 0.5 mm thick brain tumor sample. The image plane is located at a 20 μm depth from the surface. a) SRH overview image. b) Zoom into the sub-cellular detail. Pixel dwell time: 16 μs. Total image acquisition time: 9 min for 1 mm× 1.2 mm and 5120× 6144 pixel. The power levels at the samples were 20 mW and 35 mW (90 mW in total) for the pump and Stokes beams, respectively. The black and green scale bars correspond to 200 μm and 50 μm, respectively.

polymorphism. Overall, the diagnosis of an adenocarcinoma is readily established from this observation which is defined as a malignant neoplasia derived from an epithelial tissue featuring glandular origin. Since the normal histology of the brain parenchyma does not include glandular epithelium, this tumor necessarily corresponds to the dissemination of an adenocarcinoma located elsewhere in the body. This final diagnosis of metastatic adenocarcinoma indicates the requirement for immediate follow-up investigations in order to find and treat the patient's primary tumor. Thus, Fig. 2 and its wealth of information confirms that our setup is well suited for the investigation of biopsies with the potential advantage of saving time compared to conventional dye-based HE-staining as no slicing of the sample is required. Ideally, SRH-imaging of freshly excised tissue blocks would be performed directly within the operation theatre to minimize the time lapse between the iterative tissue removal and its diagnosis using a miniaturized version of our 3-color laser system.

As a second demanding task we selected imaging of deuterated bacteria - see Fig. 3. It was recently outlined that antibiotic susceptibility testing (AST) can be performed by monitoring the metabolic incorporation of deuterated glucose (glucose-d_7) to reduce the time for the determination of antibiotic resistances from 16 h to 0.5 h [26]. SRS imaging of deuterated bacteria, however, is challenging due to the samples' size which is generally below the focal volume of the excitation point spread function (PSF). Further, the concentration of the C-D molecular groups incorporated into the bacteria is low, so that even weak artifacts (thermal lensing, cross phase modulation, multi-photon absorption) may dominate the contrast and lead to wrong conclusions. Consequently, meaningful SRS C-D imaging of bacteria, does not only require a high-power shot-noise-limited system with high spatial resolution but also a reference channel to remove any background. For this purpose, the OPO was tuned to 846 nm to acquire simultaneously the in- and off-resonance SRS-image of C-D-groups at 2149 cm^{-1}

Biomedical Optics EXPRESS

and 2054 cm^{-1}, respectively, of *Staphylococcus epidermidis*. The latter were cultured either in a medium containing 2% of glucose-d_7 (deuterated) or 2% of D-glucose (non deuterated). For the experiment, we mixed bacteria nourished with a deuterated and non-deuterated diet in the ratio 2:1. From Fig. 3 a the presence of artifacts is evident which are unrelated to the SRS-contrast. Thus, the off-resonant (Fig. 3(a) image was subtracted from the resonant image of the C-D-groups (Fig. 3(b) to provide a background free SRS image displayed in Fig. 3(c). Simultaneous imaging of CH_3- (Fig. 3(d) and CH_2-groups (not shown), enables to separate the two populations of deuterated and non-deuterated bacteria as evident from Fig. 3(e) and the intensity profile in Fig. 3(f).

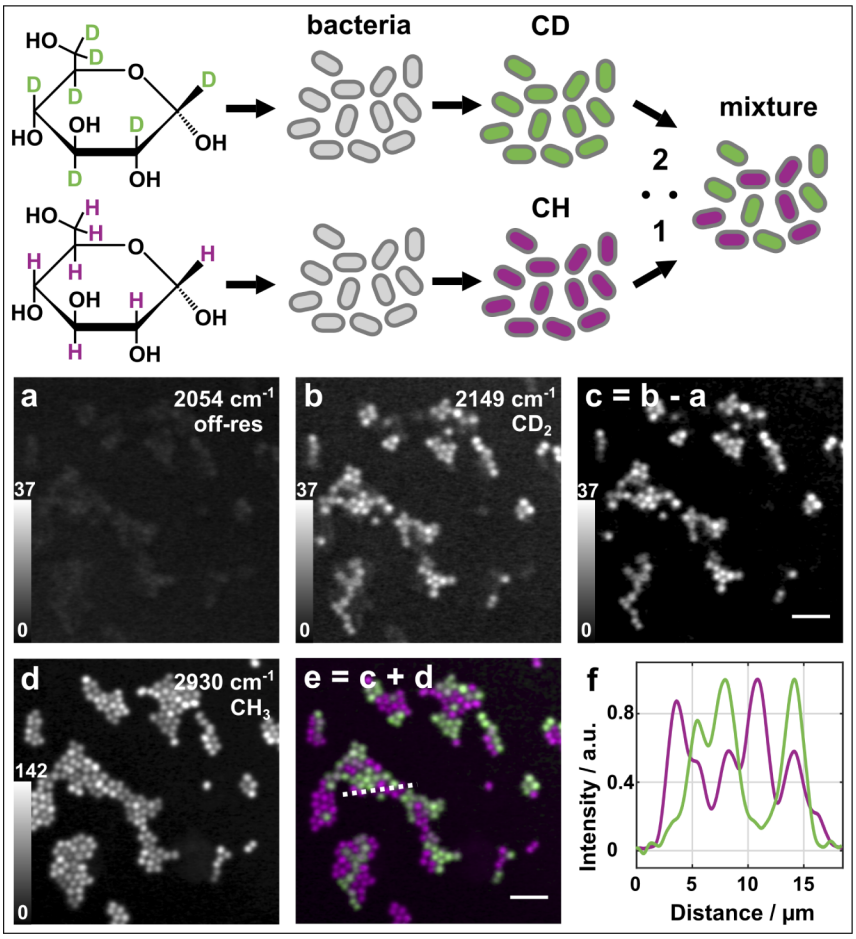

Fig. 3. Dual-color SRS imaging of *S. epidermidis* bacteria. a) Off-resonance SRS image at 2054 cm^{-1}. b) Resonant SRS image of C-D groups at 2149 cm^{-1}. c) Result of the subtraction of 2149 cm^{-1}-2054 cm^{-1} (Subfig. b and a). d) Resonant SRS image of CH_3 groups at 2940 cm^{-1}. e) Composite image of Subfig. c (green) and d (magenta) corresponding to the C-D and CH_3 groups, respectively. f) SRS intensity profile along the dotted white line in e). Pixel dwell time for C-D in- and off-resonance: 60 µs, and for C-H resonances: 20 µs. Scale bar: 10 µm. Acquisition time for C-D in- and off-resonance: 54s, and for C-H resonances: 18s.

C-D imaging within bacteria certainly demands a high sensitivity SRS system but not necessarily a high imaging speed since the bacteria are immobile and the essential information can be retrieved already within a rather limited field-of-view. The situation changes once one

Biomedical Optics EXPRESS

is interested in larger 3D-structures that are alive rendering high-speed imaging a fundamental requirement. To highlight the merits of high velocity dual-color SRS imaging we selected the wing imaginal disc of Drosophila melanogaster. The wing imaginal disc was dissected from a 5 days old larva that had been fed with deuterated yeast (cultured with 50% of D_2O in PDB medium) for 2 days prior to imaging. Though the wing disc was excised from the larva, its cells

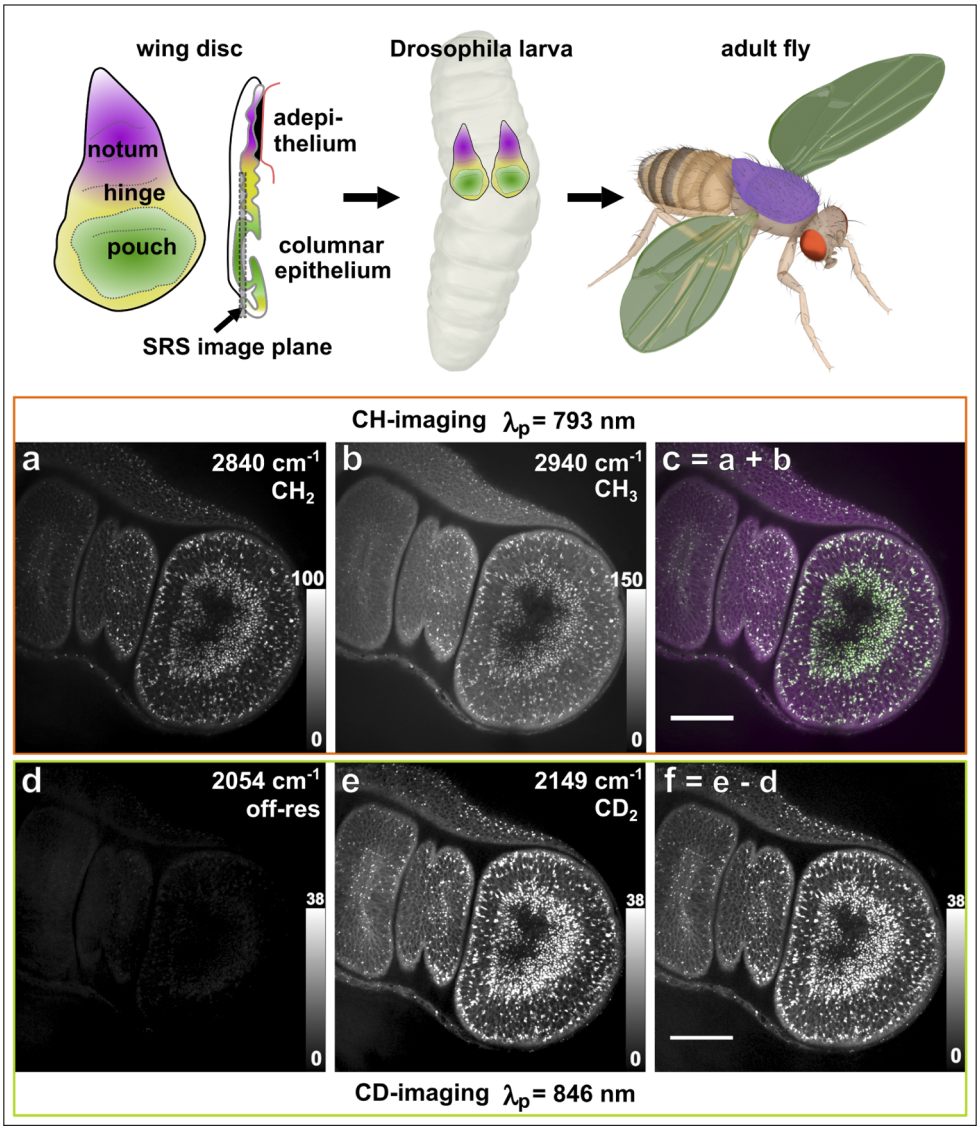

Fig. 4. Dual-color SRS imaging of a dissected wing imaginal disc of a *Drosophila* larva. a) CH_2 image acquired at 2840 cm^{-1}. b) CH_3 image acquired at 2940 cm^{-1}. c) Composite image of Subfig. a (green) and b (magenta) corresponding to the CH_2 and CH_3 groups respectively. d) Off-resonant SRS image at 2054 cm^{-1}. e) Resonant SRS image of C-D groups at 2149 cm^{-1}. f) Result of subtraction of 2149 cm^{-1}-2054 cm^{-1} (Subfig. e and d). Pixel dwell time for C-D in- and off-resonance: 5 µs, and for C-H resonances: 3 µs. Scale bar: 100 µm. Acquisition time for C-D in- and off-resonances: 21s, and for C-H resonances: 13s.

Biomedical Optics EXPRESS

are alive. They still proliferate and reshape constantly the structure of the superordinate organ. More precisely, the Drosophila wing imaginal disc consists of a simple epithelial cell sheet inside the developing larva. In the course of metamorphosis, strong morphogenetic forces distributed across the tissue will change the shape of the cell sheet such that different regions of the wing disc develop into the adult thorax, hinge and wing (see cartoon in Fig. 4). Over the years, the wing imaginal disc has proved to be a model of great importance to dissect the molecular pathways that underlie genetic patterning and growth, many of which are conserved throughout the animal kingdom [27]. Many questions remain as to how the information born by genetic patterning are decoded to instruct growth of the tissue. Notably, the biochemist community lacks a methods to map in a quantitative manner, and at high spatio-temporal resolution, the metabolic activity associated with growth. SRS-imaging of C-D labeled tissues may solve this issue by providing insights into the local distribution of the deuterium incorporation, which was reported to be in close relation to the biosynthetic activity [28].

Figure 4(a) and (b) display the wing discs investigated at 2840 cm^{-1} (CH_2) and 2940 cm^{-1} (CH_3) (overlap in Fig. 4(c)). The resulting image provides a large-scale view of the imaginal disc with enough resolution to discern individual cell membranes as well as an abundant pool of lipid droplets within the cells. The same wing disc was imaged in C-D vibrational range. The C-D signal was retrieved from the difference of the in-resonance (2149 cm^{-1}) and off-resonance (2054 cm^{-1}) as outlined in Fig. 4(d), (e) and (f). Highlighting the same pool of proteins, cell membrane and lipid droplets as in the C-H vibrational range, the analysis of C-D images opens the possibility to measure a detailed map of anabolic activity within the *Drosophila* wing imaginal disc. Thus, we conclude that the presented dual-vibrational SRS system balances nicely the demand for the highest possible imaging speed or sensitivity with the minimum amount of spectral information that is required to acquire background free images whose image brightness is proportional to the concentration of the targeted molecular group.

4. Conclusion

We presented a dual-color shot noise limited SRS imaging system with more than 200 mW per beam that allows for simultaneously SRS imaging of two distinct vibrational chemical bonds. Four ultra-steep dielectric long-pass filter were used to generate two 100 cm^{-1} separated ps Stokes beams from a 15 nm (FWHM) spectral bandwidth fs-pulse. The remainder of the latter provided sufficient power to pump an OPO that enables for wide-range tuning of the SRS pump beam while still preserving a compact footprint for the overall system. We demonstrated virtual stimulated Raman histology imaging at 20 µm depth through a 0.5 mm thick human brain cancer sample with 16 µs pixel dwell time and medium power levels at the biopsy (90 mW). Furthermore, we exemplified the relevance of the dual-color SRS system to remove SRS artifacts in sub-focal-volume partially deuterated bacteria. Finally, we showed C-H and C-D vibrational dual-color SRS imaging of the wing imaginal disc of *Drosophila* larvae. The newly developed shot noise limited SRS source reduces significantly the cost as compared to a two OPOs system and can be integrated into one affordable commercial system lowering the entry-barrier to fast and efficient vibrational imaging for research and medical applications.

Funding. INSERM (18CP128-00, PC201508); Agence Nationale de la Recherche (ANR-10-INSB-04-01, ANR-11-INSB-0006, ANR-16-CONV-0001); Région Sud; Institut National Du Cancer; Cancéropôle Provence-Alpes-Côte d'Azur; A*Midex (ANR-11-IDEX-0001-02); Aix-Marseille Université (A-M-AAP-ID-17-13-170228-15.22-RIGNEAULT); Centre National de la Recherche Scientifique.

Acknowledgements. We like to thank Flora Poizat from Institut Paoli-Calmettes (Marseille) for providing the frozen human biopsies.

Ethics. All human samples used in this study are coming from the Bio-Bank from 'Assistance Publique des hopitaux de Marseille (AP-HM)' with informed consent obtained from all participants.

Disclosures. The authors declare no conflict of interest.

Biomedical Optics EXPRESS

Data availability. The data that support the findings of this study are available from the corresponding author upon reasonable request.

Supplemental document. See Supplement 1 for supporting content.

References

1. C. W. Freudiger, W. Min, B. G. Saar, S. Lu, G. R. Holtom, C. He, J. C. Tsai, J. X. Kang, and X. S. Xie, "Label-free biomedical imaging with high sensitivity by stimulated raman scattering microscopy," Science **322**(5909), 1857–1861 (2008).
2. P. Nandakumar, A. Kovalev, and A. Volkmer, "Vibrational imaging based on stimulated Raman scattering microscopy," New J. Phys. **11**(3), 033026 (2009).
3. Y. Ozeki, F. Dake, S. Kajiyama, K. Fukui, and K. Itoh, "Analysis and experimental assessment of the sensitivity of stimulated Raman scattering microscopy," Opt. Express **17**(5), 3651 (2009).
4. H. Rigneault and P. Berto, "Tutorial: coherent Raman light matter interaction processes," APL Photonics **3**(9), 091101 (2018).
5. P. Berto, E. R. Andresen, and H. Rigneault, "Background-free stimulated Raman spectroscopy and microscopy," Phys. Rev. Lett. **112**(5), 053905 (2014).
6. A. Lombardini, P. Berto, J. Duboisset, E. R. Andresen, S. Heuke, E. Büttner, I. Rimke, S. Vergnole, V. Shinkar, P. de Bettignies, and H. Rigneault, "Background-suppressed SRS fingerprint imaging with a fully integrated system using a single optical parametric oscillator," Opt. Express **28**(10), 14490 (2020).
7. S. Heuke, A. Lombardini, E. Büttner, and H. Rigneault, "Simultaneous stimulated Raman gain and loss detection (SRGAL)," Opt. Express **28**(20), 29619–29630 (2020).
8. Y. Ozeki, W. Umemura, Y. Otsuka, S. Satoh, H. Hashimoto, K. Sumimura, N. Nishizawa, K. Fukui, and K. Itoh, "High-speed molecular spectral imaging of tissue with stimulated raman scattering," Nature Photonics **6**(12), 845–851 (2012).
9. K. Seto, Y. Okuda, E. Tokunaga, and T. Kobayashi, "Development of a multiplex stimulated raman microscope for spectral imaging through multi-channel lock-in detection," Review of Scientific Instruments **84**(8), 083705 (2013).
10. J. Réhault, F. Crisafi, V. Kumar, G. Ciardi, M. Marangoni, G. Cerullo, and D. Polli, "Broadband stimulated raman scattering with Fourier-transform detection," Opt. Express **23**(19), 25235 (2015).
11. D. Fu, F.-K. Lu, X. Zhang, C. Freudiger, D. R. Pernik, G. Holtom, and X. S. Xie, "Quantitative chemical imaging with multiplex stimulated raman scattering microscopy," J. Am. Chem. Soc. **134**(8), 3623–3626 (2012).
12. C.-S. Liao, P. Wang, P. Wang, J. Li, H. J. Lee, G. Eakins, and J.-X. Cheng, "Spectrometer-free vibrational imaging by retrieving stimulated raman signal from highly scattered photons," Sci. Adv. **1**(9), e1500738 (2015).
13. D. Zhang, M. N. Slipchenko, D. E. Leaird, A. M. Weiner, and J.-X. Cheng, "Spectrally modulated stimulated raman scattering imaging with an angle-to-wavelength pulse shaper," Opt. Express **21**(11), 13864 (2013).
14. R. He, Y. Xu, L. Zhang, S. Ma, X. Wang, D. Ye, and M. Ji, "Dual-phase stimulated Raman scattering microscopy for real-time two-color imaging," Optica **4**(1), 44 (2017).
15. W. Yang, A. Li, Y. Suo, F.-K. Lu, and X. S. Xie, "Simultaneous two-color stimulated Raman scattering microscopy by adding a fiber amplifier to a 2 ps OPO-based SRS microscope," Opt. Lett. **42**(3), 523 (2017).
16. S. Heuke, B. Sarri, X. Audier, and H. Rigneault, "Simultaneous dual-channel stimulated raman scattering microscopy demultiplexed at distinct modulation frequencies," Opt. Lett. **43**(15), 3582 (2018).
17. D. A. Orringer, B. Pandian, Y. S. Niknafs, T. C. Hollon, J. Boyle, S. Lewis, M. Garrard, S. L. Hervey-Jumper, H. J. L. Garton, C. O. Maher, J. A. Heth, O. Sagher, D. A. Wilkinson, M. Snuderl, S. Venneti, S. H. Ramkissoon, K. A. McFadden, A. Fisher-Hubbard, A. P. Lieberman, T. D. Johnson, X. S. Xie, J. K. Trautman, C. W. Freudiger, and S. Camelo-Piragua, "Rapid intraoperative histology of unprocessed surgical specimens via fibre-laser-based stimulated Raman scattering microscopy," Nat Biomed Eng **1**(2), 0027 (2017).
18. B. Sarri, R. Canonge, X. Audier, E. Simon, J. Wojak, F. Caillol, C. Cador, D. Marguet, F. Poizat, M. Giovannini, and H. Rigneault, "Fast stimulatedRaman and second harmonic generation imaging for intraoperative gastro-intestinal cancer detection," Sci Rep **9**(1), 10052 (2019).
19. B. Sarri, F. Poizat, S. Heuke, J. Wojak, F. Franchi, F. Caillol, M. Giovannini, and H. Rigneault, "Stimulated Raman histology: one to one comparison with standard hematoxylin and eosin staining," Biomed. Opt. Express **10**(10), 5378 (2019).
20. T. C. Hollon, B. Pandian, A. R. Adapa, E. Urias, A. V. Save, S. S. S. Khalsa, D. G. Eichberg, R. S. D'Amico, Z. U. Farooq, S. Lewis, P. D. Petridis, T. Marie, A. H. Shah, H. J. L. Garton, C. O. Maher, J. A. Heth, E. L. McKean, S. E. Sullivan, S. L. Hervey-Jumper, P. G. Patil, B. G. Thompson, O. Sagher, G. M. McKhann, R. J. Komotar, M. E. Ivan, M. Snuderl, M. L. Otten, T. D. Johnson, M. B. Sisti, J. N. Bruce, K. M. Muraszko, J. Trautman, C. W. Freudiger, P. Canoll, H. Lee, S. Camelo-Piragua, and D. A. Orringer, "Near real-time intraoperative brain tumor diagnosis using stimulated raman histology and deep neural networks," Nat Med **26**(1), 52–58 (2020).
21. X. Audier, S. Heuke, P. Volz, I. Rimke, and H. Rigneault, "Noise in stimulated raman scattering measurement: from basics to practice," APL Photonics **5**(1), 011101 (2020).
22. T. Hellerer, A. M. Enejder, and A. Zumbusch, "Spectral focusing: High spectral resolution spectroscopy with broad-bandwidth laser pulses," Appl. Phys. Lett. **85**(1), 25–27 (2004).
23. C. W. Freudiger, W. Yang, G. R. Holtom, N. Peyghambarian, X. S. Xie, and K. Q. Kieu, "Stimulated raman scattering microscopy with a robust fibre laser source," Nature Photonics **8**(2), 153–159 (2014).

Biomedical Optics EXPRESS

24. S. Brustlein, P. Ferrand, N. Walther, S. Brasselet, C. Billaudeau, D. Marguet, and H. Rigneault, "Optical parametric oscillator-based light source for coherent raman scattering microscopy: practical overview," J. Biomed. Opt. **16**(2), 021106 (2011).
25. T. A. Pologruto, B. L. Sabatini, and K. Svoboda, "ScanImage: flexible software for operating laser scanning microscopes," BioMed Eng OnLine **2**(1), 13 (2003).
26. W. Hong, C. W. Karanja, N. S. Abutaleb, W. Younis, X. Zhang, M. N. Seleem, and J.-X. Cheng, "Antibiotic susceptibility determination within one cell cycle at single-bacterium level by stimulated raman metabolic imaging," Anal. Chem. **90**(6), 3737–3743 (2018).
27. J. V. Beira and R. Paro, "The legacy of *Drosophila* imaginal discs," Chromosoma **125**(4), 573–592 (2016).
28. L. Shi, C. Zheng, Y. Shen, Z. Chen, E. S. Silveira, L. Zhang, M. Wei, C. Liu, C. de Sena-Tomas, K. Targoff, and W. Min, "Optical imaging of metabolic dynamics in animals," Nat Commun **9**(1), 2995 (2018).